Smart Infrastructure and Construction **00**, 1–15 [http://dx.doi.org/10.1680/jsmic.XX.XXXXX]

Pavement degradation: a city-scale model for San Francisco

BINGYU ZHAO*§, ELISABETE SILVA (PHD)†, KENICHI SOGA (FRENG, FICE)‡

Data from long-term systematic pavement condition surveys provide the opportunities to better understand the pavement degradation process. To provide more accurate predictions on future pavement conditions, spatial conditions are incorporated into degradation models of pavements in this paper. Long-term, city-scale pavement condition data from the San Francisco open data portal are used to test and guide model development. Spatial and non-spatial degradation models are developed and compared, with parameter estimations carried out using the Bayesian approach. Specifically, the Integrated Nested Laplace Approximation (INLA) method is used for the Bayesian regression. It was found that: (1) the non-spatial model including only coarse categories of pavement types is too simple to provide a good fit to the data; (2) for models with fine categories (individual street segments), the spatial model is more preferable than the non-spatial model due to its lower Deviance Information Criterion (DIC) and slightly smaller fitting and testing errors; (3) only the spatial model can reveal the spatial clustering of streets where high/low degradation rates concentrate.

(Manuscript submitted on March 6, 2018; Main text: 4,950 words; 12 figures; 4 tables.)

KEYWORDS: City-scale simulations and data analytics, Data analytics for infrastructure, Pavement deterioration modelling, Spatial model, INLA *Smart Infrastructure and Construction*

INTRODUCTION

Thanks to the recent advancements in pavement condition monitoring and management, pavement condition data are becoming available at increasingly large spatial scales and high spatial resolutions (Benbow *et al.*, 2017; Wang *et al.*, 2014; Zhao & Nagayama, 2017). This provides both opportunities and challenges for pavement management: the opportunities are to understand network-wide condition change and maintenance needs at high spatio-temporal resolution. While the challenges are to analyse large amounts of spatio-temporal data in an efficient manner and identify meaningful and usable quantifications for pavement maintenance management.

Spatial and spatio-temporal data are widely used in geographic and urban-related studies, such as ecology, meteorology, criminology, land use and transportation (Aljoufie *et al.*, 2013; Baller *et al.*, 2001; Handcock & Wallis, 1994; Lichstein *et al.*, 2002; Silva & Clarke, 2005). In pavement management, there are also works addressing various spatial aspects and proposing methods for visualization, spatial characters quantification, missing data imputation and decision making (Chen *et al.*, 2014; Saliminejad & Gharaibeh, 2012). But direct applications of spatial and spatio-temporal modelling for infrastructure management are still limited (Anyala *et al.*, 2014; Deshmukh, 2010; Ortiz-García *et al.*, 2006).

This paper incorporates both spatial and temporal dimensions into pavement degradation modelling. It is organised as the following: first the background is introduced about the necessity of system-wide understanding from pavement asset management perspective. Next, data from the case study area are presented, together with descriptions of the data cleaning procedures. In the methodology section, the fundamentals of spatial models are reviewed and a multi-level spatial pavement degradation model is proposed. Also in this section, the Integrated Nested Laplace Approximation (INLA) is introduced, which is adopted for parameter inference in this study due to its computational efficiency (Rue *et al.*, 2009). Two non-spatial models and one spatial model with spatially correlated degradation rates are designed to represent a variety of pavement degradation modelling strategies. The results of these three models are compared in terms of their fitting and predicting abilities, the Deviance Information Criterion (DIC) and the spatial representations. Although pavement condition is modelled as degrading linearly with age, this can be modified in the future to include higher order terms. The aim of this work is to demonstrate the technique, as well as the providing pros and cons of spatial pavement degradation models, which future studies can benefit from when choosing between alternative modelling strategies. The paper is concluded with discussions about the values and limitations of this study, and plans for future work.

Manuscript received on March 6, 2018
* PhD student, Department of Engineering, University of Cambridge, Cambridge, CB2 1PZ, UK (https://orcid.org/0000-0002-2369-7731);
† Reader, Department of Land Economy, University of Cambridge, Cambridge, CB3 9EP, UK (https://orcid.org/0000-0002-5816-6447);
‡ Chancellor's Professor, Department of Civil and Environmental Engineering, University of California, Berkeley, 94707, USA (https://orcid.org/0000-0001-5418-7892);
§ Corresponding author. Email: bz247@cam.ac.uk

BACKGROUND

Pavement asset managers have always been seeking methods that help with the decisions of when and where to carry out maintenance (Golabi *et al.*, 1982; Ferreira *et al.*, 2002; Wu *et al.*, 2008; Gao & Zhang, 2012; Zhang *et al.*, 2012). In the past, such decisions were largely hindered by the scarcity of data: usually pavement performance models or insights were based on data collected at a small scale, thus not representative enough given the natural variability of pavement degradation process (Johnson & Cation, 1992; Nunez & Shahin, 1986). The situation improves recently as in many places, pavement inspections are carried out more frequently system-wide (McQueen & Timm, 2005; Haider *et al.*, 2010; Sadeghi *et al.*, 2017). However, when it comes to maintenance planning, there are still many difficulties in producing a reliable pavement condition prediction model, especially with the strong presence of measurement errors inherent to visual surveys and a lack of knowledge on crucial degradation-affecting factors (e.g., construction quality, history of minor maintenance activities), as encountered in this study.

As a result, to address the issue of "imperfect data", additional structures in the data should be considered as

useful information, which will hopefully bring about more insights. There have been several studies incorporating the underlying hierarchies of the pavement degradation process. For example, a model is proposed by Anyala *et al.* (2014) to assess the impact of climate change on pavement rutting. In this hierarchical Bayesian model, Level 1 parameters govern the degradation process of each surface group while at the same time being constrained by Level 2 parameters (network-level). This hierarchical structure is used to reduce the parameter estimation uncertainties. In another study (Alaswadko *et al.*, 2019), roughness (IRI) was modelled in a linear hierarchical manner, reflecting the structured variations of pavement IRI by each section, highway and road classes. These existing studies mainly rely on the known hierarchical structures of the street network as additional information. While in this study, it is shown that the similar hierarchical modelling approach can be applied in a more general manner, taking advantage of the natural spatial structures of the street network.

DATA

Pavement condition data used in this study are published by the San Francisco Department of Public Work on DataSF (data.sfgov.org) under the Open Data Commons Public Domain Dedication and License (Open Data Commons, 2009). It provides historical and current information on the Pavement Condition Index (PCI) of more than 12,000 street segments in the city (Figure 1). PCI is a numerical scale from 0-100 that is used to represent the general condition of pavement, with 0 being badly deteriorated roads and 100 representing brand new conditions. It was originated in the U.S. in the late 1970s and is still widely used for pavement condition assessment (Shahin *et al.*, 1978; Shahin & Kohn, 1982).

Table 1 offers a glimpse of the dataset by showing the records belonging to street segment 'CNN100000' at different times. The pavement condition data are collected by the SF DPW using visual surveys and they have been used for asset management, decision making as well as publicity purposes. For example, they are used to demonstrate the pavement condition changes on a yearly basis for each city and county in the Bay Area (Vital Signs, 2017), to assess the outcome of major infrastructure investments (SF Public Works, 2017) and so on. As for pavement performance forecasting, the data are most notably used in the calibration of the pavement performance model in StreetSaver, a Pavement Management Software (PMS) developed by the Bay Area MTC and used by many local agencies in the west coast of the US. The StreetSaver model utilizes a family of deterministic S-shaped curves to predict pavement deterioration as a function of time, with model parameters obtained from weighted least square regression (Deshmukh, 2010). To further improve the deterministic model in StreetSaver, Ramirez-Flores & Chang-Albitres (2012) proposed a stochastic model that projects pavement conditions as a probability distribution. However, both of these two existing studies categorised the city-scale data by pavement types and did not consider the possible spatial correlations between individual pavement sections.

Although the earliest record date is in 1947, most record dates are after 1992 (Figure 2(a)). Initial explorations of the dataset also show that the PCI records before 1995 may not be fully reliable, since for more than 70% of the street segments, the PCI values from 1992 to 1994 are exactly the same (see an example of such duplicates in Figure 2(b)). As a result, only data collected in and after 1995 are used for further analysis.

Aging is a major factor that leads to the degradation of pavement conditions (Paterson, 1987). In the San Francisco PCI dataset, only curb-to-curb maintenance projects are recorded. Based on these maintenance records, pavement "age" since last maintenance is calculated and used as an explanatory variable in degradation models. As only maintenance records can help to determine the "age" of the pavements, PCI records without clear previous maintenance dates are thus removed. A scatter plot of pavement segments' PCI versus age based on the whole dataset at this stage is given by Figure 3. As there are overlapping data points, all data points are made semi-transparent. Thus, the darker the colour, the more points are located at a position.

Next, some obvious outliers of the PCI records are filtered out. Outliers are defined as survey records with an annual change of PCI larger than 40 (Figure 4(a)). Besides, as only curb-to-curb maintenance works are documented, it means that small scale road works, such as patching or pothole filling, are not reflected in the dataset. To mitigate the influence of these missing maintenance records on inferring the degradation rates, streets that show significant improvements (PCI larger than 20 per year) without maintenance have their conditions shifted back to their previous values (Figure 4(b)).This allows the examination of the general degradation trend of a particular road segment between major maintenance events. Survey errors and the absence of some maintenance records are two major limitations in the data. These are two pervasive issues in pavement condition databases and need to be solved, e.g., through automated pavement condition surveys or better documentation of road works, for better degradation analysis and pavement asset management.

Traffic, material, climate and construction quality also play important roles in the pavement degradation process (Ferreira *et al.*, 2011; Morosiuk *et al.*, 2004). However, not all of these data are well documented or easily accessible. In this study, only the pavement material types and road functional classes are available. Table 2 summarises the number of street segments in each material and functional class category. It can be seen that the majority of streets are asphalt concrete overlaid on top of Portland cement concrete. These categorical characters will be taken into account in the subsequent degradation modelling.

After the above basic data cleaning and processing, 8218 street segments and 49542 PCI records remain in the dataset. This equals to about 5 observations per street segment during the study period from 1995 to 2017 (Figure 5). Figure 6 shows the PCI value against pavement age of the cleaned dataset, grouped by pavement category. As in Table 2, the majority of the pavements have the surface type "C" (asphalt concrete overlaid on top of Portland cement concrete), while few segments have the surface type "O" (asphalt concrete overlaid on top of asphalt concrete). Also from Figure 6, it can be seen that there is a significant variability in pavement degradation trends even for streets belonging to the same category. Simple degradation models based on pavement categories are unlikely to work well in producing accurate predictions on pavement conditions.

The nearly 50,000 pavement condition records from the cleaned dataset are randomly split into a training set and a testing set. The training set consists of 39635 records, or roughly 80% of the whole set. The testing set contains the rest of the 9907 records. In the further analysis, the training set will be used to obtain model coefficients and to evaluate how well the models do in fitting a specific large dataset; while the testing set will be used to check the generality, i.e., how well the models perform when tested on data unseen.

METHODOLOGY

With pavement age (continuous), surface type (categorical) and street functional class (categorical) as the explanatory

Table 1. Pavement condition records of a street segment

CNN	Street Name	From Street	To Street	Functional Class	Surface Type	PCI Score	PCI Change Date	Maintenance or Survey
100000	01ST ST	Market St	Stevenson St	Arterial	C	100	05/09/2001 12:00:00 AM	Treatment
100000	01ST ST	Market St	Stevenson St	Arterial	C	100	11/19/2002 12:00:00 AM	Survey
100000	01ST ST	Market St	Stevenson St	Arterial	C	100	11/16/2005 04:50:06 PM	Survey
100000	01ST ST	Market St	Stevenson St	Arterial	C	100	07/26/2007 04:21:27 PM	Survey
100000	01ST ST	Market St	Stevenson St	Arterial	C	93	08/10/2009 03:43:09 PM	Survey
100000	01ST ST	Market St	Stevenson St	Arterial	C	73	12/23/2010 01:37:36 PM	Survey
100000	01ST ST	Market St	Stevenson St	Arterial	C	56	01/08/2013 03:18:02 PM	Survey
100000	01ST ST	Market St	Stevenson St	Arterial	C	61	11/25/2014 02:17:39 AM	Survey

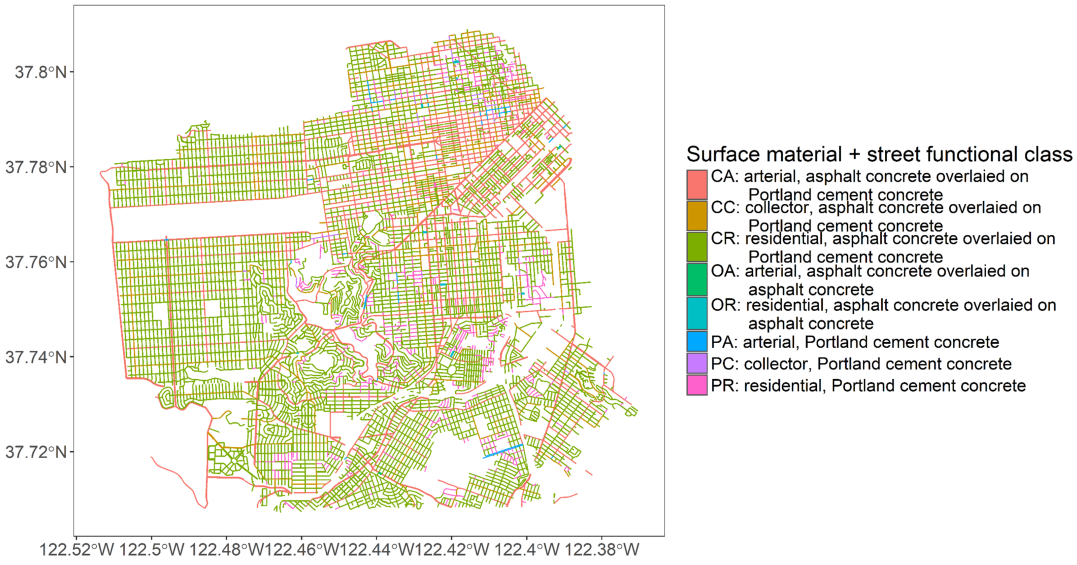

Fig. 1. Street network in San Francisco, colored by surface type and functional class categories.

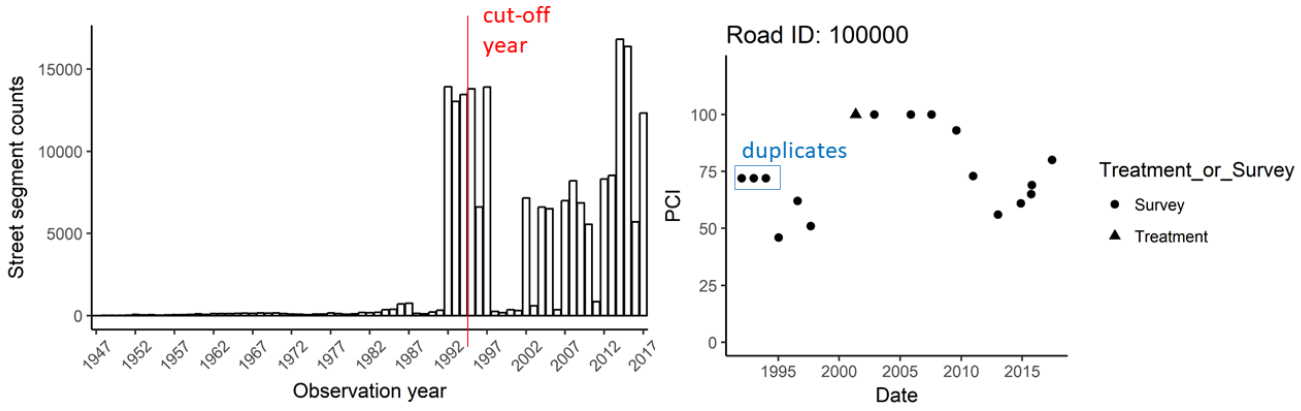

Fig. 2. PCI records. (a) A histogram of the observation dates; (b) An example of duplicated PCI values in 1992-1994.

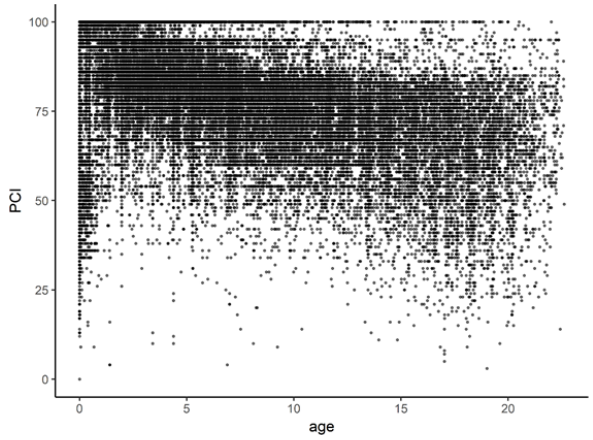

Fig. 3. A scatter plot of pavement section's PCI versus age.

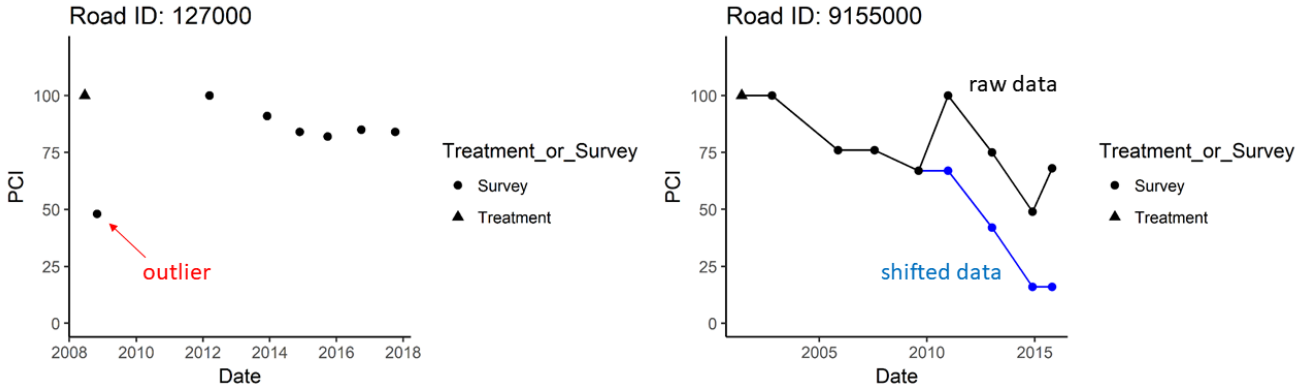

Fig. 4. Data cleaning examples. (a) Removing outliers; (b) Handling potential missing maintenance records.

Table 2. Pavement categories and numbers of street segments in each category.

Street segment counts (in brackets: abbreviations of category types)	Arterial (A)	Collector (C)	Residential/Local (R)
Portland cement concrete (P)	99 (PA)	82 (PC)	1192 (PR)
Asphalt concrete overlaied on asphlat concrete (O)	8 (OA)	NA	40 (OR)
Asphlat concrete overlaid on Portland cement concrete (C)	13817 (CA)	3780 (CC)	30524 (CR)

variables, a simple and straightforward way to model pavement degradation is: divide all observations in the training data set into categories based on their surface types and functional classes, then build a regression model for pavement age and condition for each category. However, as there are only 8 surface type and functional class combinations (Table 2), the categorisation used in this simple model may not be sufficient to represent the diverse pavement characteristics in reality. It is also possible to test the other extreme by considering each street itself as a category and grouping the observed data by street IDs. This allows the individual characters of each street (e.g., climate, geology, construction quality, traffic load, etc.) to be fully captured and represented. However, the numbers of parameters involved in this model will also be large and may lead to overfitting. A third alternative is to choose a medium cluster size, smaller than a street type/functional class category, but larger than an individual street. Spatial modelling offers this capability by incorporating dependencies between neighbouring spatial units and is chosen as the third modelling strategy in this paper.

The Spatial Model

Spatial model allows smoothly varying coefficients across the entire study area. A simple way to incorporate spatial relationships in a model is to include the longitude and latitude coordinates as model predictors and fit a trend surface. However, such models can only capture global trends if not using high order terms (Lichstein *et al.*, 2002). To represent localised interactions, model structures such as the Geographically Weighted Regression (GWR), Simutaneous Autoregression (SAR) and Conditional Autoregression (CAR) are more suitable. These model structures consider spatial dependencies between neighbours by imposing constraints on the values (or residuals) of neighbouring sites (Dormann *et al.*, 2007). Readers can refer to Jahanbakhsh *et al.* (2016) for a SAR model that predict pavement conditions with spatial and temporal lags. This study is designed to model street-specific degradation rates as the average of neighbouring rates, so an intrinsic conditional autoregressive (iCAR) 'Besag' model becomes a natural choice (Besag *et al.*, 1991; Blangiardo *et al.*, 2013; Lavine & Hodges, 2012).

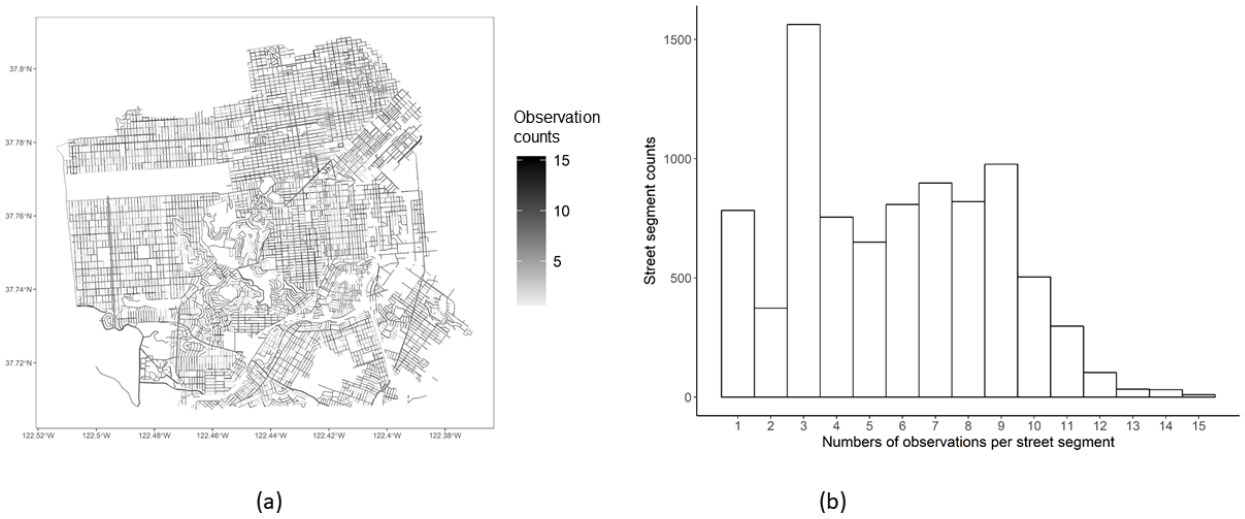

Fig. 5. Numbers of observations per street segment. (a) A spatial view: the darker the street, the more observations available; (b) The histogram.

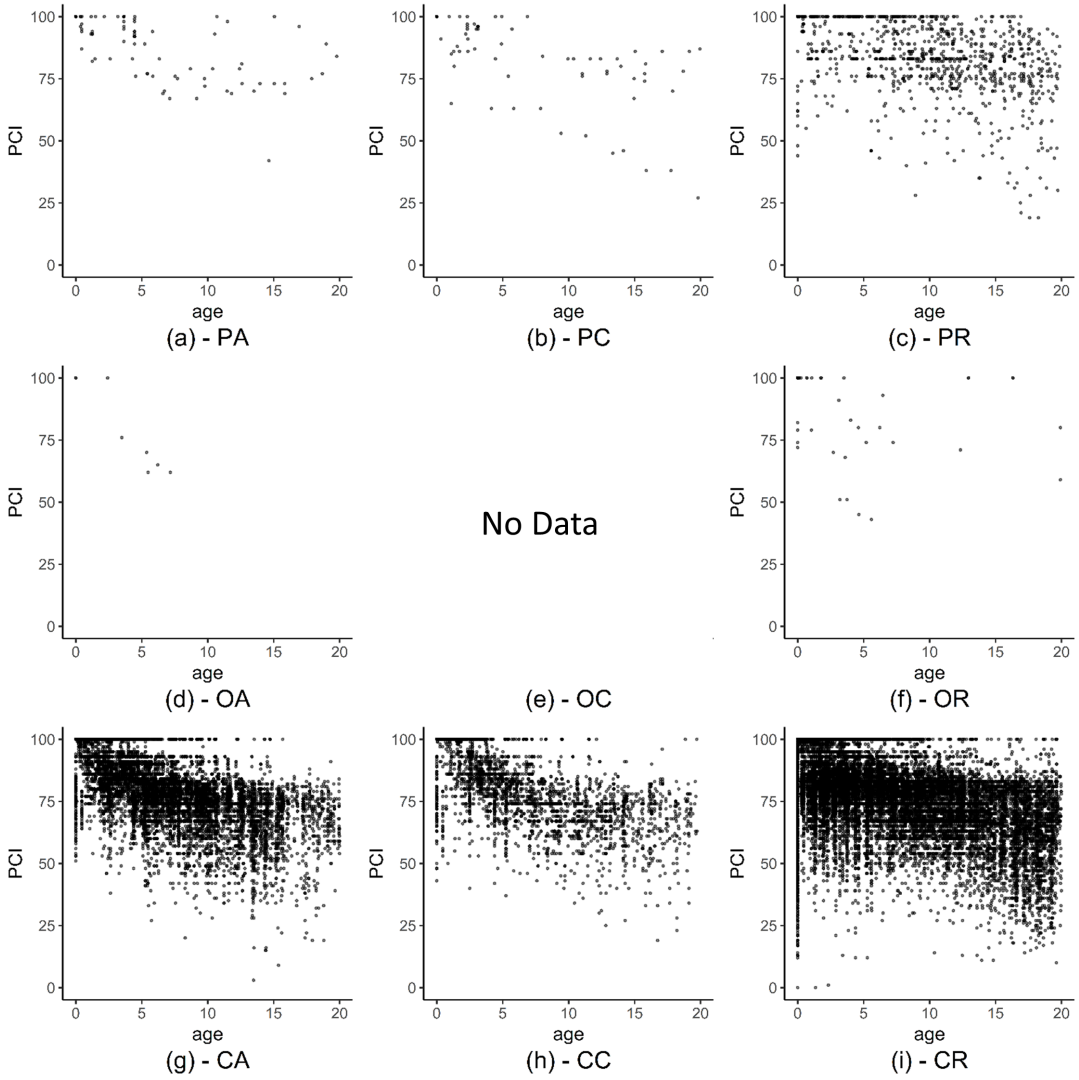

Fig. 6. PCI versus pavement age, grouped by pavement category. Refer to Table 2 for meanings of abbreviations.

Pavement degradation with spatial effects can be formulated as the following multi-level model (Blangiardo & Cameletti, 2015; Rue *et al.*, 2009): the first step is to model the distribution of the observations:

$$y_{ik} \sim N(\eta_{ik}, \frac{1}{\tau_g}) \tag{1}$$

where y_{ik} is the k-th observed PCI at street i, given that most of the street segments have more than one record in the past 20 years (Figure 5). y_{ik} is assumed to follow a normal distribution with mean η_{ik} and precision τ_g (inverse of variance). The distribution equation states that the observed PCI centres around an unobservable mean η_{ik}, plus some random deviations determined by the precision parameter τ_g. In the second step, η_{ik} is modelled by a linear combination of the explanatory variables:

$$\eta_{ik} = \alpha + \xi_i + (\beta + v_i + u_i)x_{ik} \tag{2}$$

$$\xi_i \sim N(0, \frac{1}{\tau_\xi}) \tag{3}$$

$$u_i \sim N(0, \frac{1}{\tau_u}) \tag{4}$$

$$v_i | v_{j\neq i}, \tau_v \sim N(\frac{1}{n_i}\sum_{j\sim i} v_j, \frac{1}{n_i \tau_v}) \tag{5}$$

x_{ik} is the explanatory variable (age) corresponding to observation y_{ik}. α and β are the global average intercept and age effect shared by all streets. ξ_i is the street specific variation in intercept, which itself is a random variable following a zero-mean normal distribution (Equation (3)). $\beta + v_i + u_i$ is the total street specific age effect for street i, where v_i is the spatially structured individual deviation from the mean and u_i is the unstructured part. A Besag specification is adopted for modelling v_i (Besag *et al.*, 1991; Blangiardo *et al.*, 2013): as shown in Equation (5), v_i is a Gaussian random variable whose mean equals to the average of neighbouring sites' values v_j ($j \sim i$ means i, j are neighbours) and whose precision τ_v is to be estimated from the data. n_i is the numbers of neighbours that street i has. Since v_i is only related to its neighbours, v_i and v_l are conditionally independent if i and l are not neighbours (the Markov property). So $\boldsymbol{v} = \{v_1, v_2, ...\}$ is said to be a Gaussian Markov Random Field (GMRF).

In the third step of the multi-level model, prior distributions are assigned to model parameters. Details on prior distributions will be given in the modelling section. A graphical model for the three-level spatial model is given in Figure 7(d).

Bayesian Regression using R-INLA

For multi-level models such as the one presented above, various techniques are available for parameter inference, including the maximum likelihood estimation, the Markov Chain Monte Carlo (MCMC) method and so on (Croissant *et al.*, 2008; Gelman & Hill, 2006). Rue *et al.* (2009) has demonstrated that a direct approximation based Bayesian approach, called the Integrated Nested Laplace Approximation (INLA), to be fast and sufficiently accurate for parameter inferences of spatial hierarchical models. In the preliminary stage of this study, the MCMC approach also showed promising and comparable results. Since the scope of this paper is to compare spatial and non-spatial model structures rather than the various inference methods, only INLA, the most flexible approach according the authors' experience, is adopted.

Continuing with the notation definitions in Equation (1)-(5), the task of regression is to estimate model parameters $\boldsymbol{\theta} = \{\alpha, \beta, \boldsymbol{\xi}, \boldsymbol{v}, \boldsymbol{u}\}$ and hyperparameters $\boldsymbol{\psi} = \{\tau_g, \tau_{xi}, \tau_u, \tau_v\}$ from the data. Based on the Bayes' theorem and conditional probability, the joint posterior distribution $\pi(\boldsymbol{\theta}, \boldsymbol{\psi}|\boldsymbol{y})$ is given by:

$$\pi(\boldsymbol{\theta}, \boldsymbol{\psi}|\boldsymbol{y}) \propto \pi(\boldsymbol{y}|\boldsymbol{\theta}, \boldsymbol{\psi})\pi(\boldsymbol{\theta}|\boldsymbol{\psi})\pi(\boldsymbol{\psi}) \tag{6}$$

From Equation (6), marginal posteriors of a parameter, $p(\theta_w|\boldsymbol{y})$, and a hyperparameter, $p(\psi_h|\boldsymbol{y})$, can be obtained through integration:

$$\pi(\theta_w|\boldsymbol{y}) = \int \pi(\theta_w|\boldsymbol{\psi}, \boldsymbol{y})\pi(\boldsymbol{\psi}|\boldsymbol{y})d\boldsymbol{\psi} \tag{7}$$

$$\pi(\psi_h|\boldsymbol{y}) = \int \pi(\boldsymbol{\psi}|\boldsymbol{y})d\boldsymbol{\psi}_{-h} \tag{8}$$

INLA does the above integrations through approximating the integrands with known distributions. Based on Tierney & Kadane (1986), Rue & Martino (2007) proposed the following approximation:

$$\pi(\boldsymbol{\psi}|\boldsymbol{y}) = \frac{\pi(\boldsymbol{\theta}, \boldsymbol{\psi}|\boldsymbol{y})}{\pi(\boldsymbol{\theta}|\boldsymbol{\psi}, \boldsymbol{y})} \propto \frac{\pi(\boldsymbol{\theta}, \boldsymbol{\psi}, \boldsymbol{y})}{\widetilde{\pi}_G(\boldsymbol{\theta}|\boldsymbol{\psi}, \boldsymbol{y})}\Big|_{\boldsymbol{\theta}=\boldsymbol{\theta}^*(\boldsymbol{\psi})} \tag{9}$$

where $\widetilde{\pi}_G(\boldsymbol{\theta}|\boldsymbol{\psi}, \boldsymbol{y})$ is the Gaussian approximation of $\pi(\boldsymbol{\theta}|\boldsymbol{\psi}, \boldsymbol{y})$ near its mode $\boldsymbol{\theta}^*(\boldsymbol{\psi})$. The formula is equivalent to the Laplace approximation of marginal posterior density in Tierney & Kadane (1986). Similarly, the other integrand in Equation (7) is approximated by (Rue *et al.*, 2009):

$$\begin{aligned}\pi(\theta_w|\boldsymbol{\psi}, \boldsymbol{y}) &= \frac{\pi(\theta_w, \boldsymbol{\theta}_{-w}|\boldsymbol{\psi}, \boldsymbol{y})}{\pi(\boldsymbol{\theta}_{-w}|\theta_w, \boldsymbol{\psi}, \boldsymbol{y})} \\ &\propto \frac{\pi(\boldsymbol{\theta}, \boldsymbol{\psi}, \boldsymbol{y})}{\widetilde{\pi}_G(\boldsymbol{\theta}_{-w}|\theta_w, \boldsymbol{\psi}, \boldsymbol{y})}\Big|_{\boldsymbol{\theta}_{-w}=\boldsymbol{\theta}^*_{-w}(\boldsymbol{\psi})}\end{aligned} \tag{10}$$

Substituting the integrands in Equations (7) and (8) with Equations (9) and (10), the marginal posterior distributions become integrations at a much lower dimension, which can then be solved numerically. In this study, the R package 'INLA' (www.r-inla.org) is used for the Bayesian INLA regression. Apart from the methodological references by Rue & Martino (2007) and Rue *et al.* (2009), information about INLA applications can also be found in Blangiardo *et al.* (2013) and Schrödle & Held (2011).

MODELS

As discussed in the methodology section, three pavement degradation models are designed to represent an array of modelling strategies:

- NSP-1: a non-spatial model with data divided into coarse categories based on pavement surface type and street functional class;
- NSP-2: a non-spatial model with data divided into fine categories based on street ID;
- SP: a spatial model with fine categories (i.e., fine spatial units based on street ID).

The mathematical forms for these models are given in Table 3. Directed acyclic graphic (DAG) models showing variable relationships are provided in Figure 7. For the purpose of clarity, the DAG models in Figure 7 are based on a simplified network which consists of only four road segments in two pavement categories (Figure 7(a)), as opposed to the 8218 segments and eight pavement categories (Table 2) in the real dataset. Nontheless, the simplified network and DAG models in Figure 7 are sufficient to illustrate the structures and differences of the three models.

Table 3. Models

No.	Features	Model	Definitions
NSP-1	Global level; regression by category	$y_{Ik} = \alpha_I + \beta_I x_{Ik}$	I: index for road type and functional class category y_{Ik}: k-th observation in category I x_{Ik}: corresponding pavement age for y_{Ik} α_I and β_I: regression parameters for category I
NSP-2	Street level; Spatially-unstructured intercepts and age effects	$y_{ik} = \alpha + \xi_i + (\beta + u_i)x_{ik}$ $\xi_i \sim N(0, \tau_\xi^{-1})$ $u_i \sim N(0, \tau_u^{-1})$	i: index for road segment y_{ik}: k-th observation for road i x_{ik}: corresponding pavement age for y_{ik} α and β: global average intercept and age effect ξ_i: street-level intercept deviation from α u_i: street-level age effect deviation from β τ_ξ: precision for the iid variable ξ τ_u: precision for the iid variable u
SP	Street level; Spatially-unstructured intercepts and spatially-structured age effects	$y_{ik} = \alpha + \xi_i + (\beta + u_i + v_i)x_{ik}$ $\xi_i \sim N(0, \tau_\xi^{-1})$ $u_i \sim N(0, \tau_u^{-1})$ $v_i \vert v_{j,i\neq j}, \tau \sim N(\frac{1}{n_i}\sum_{i\sim j} v_j, \frac{1}{n_i \tau_v})$	i, y_{ik}, x_{ik}, α, β, ξ_i, τ_ξ, τ_u: same as in NSP-2 u_i: the spatially-unstructured street-level age effect deviation from β v_i: the spatially-structured street-level age effect deviation from β $i \sim j$: i and j are neighbours τ_v: the precision related parameter for spatially-structured random variable v

NSP-1

NSP-1 is a simple model where pavement condition observations are divided into categories first based on the surface materials and street functional classes, as shown in Figure 6. Separately in each category, the condition degradation is modelled with a non-spatial linear form, where age is the main explanatory variable. Visually, this is equivalent to fit a linear trend to data in each cell in Figure 6. Although more complex model forms can be used, such as the non-linear trend used by the California Metropolitan Transport Commission (MTC) (Deshmukh, 2010), a linear form is a good starting point for showing the overall trend and comparing with model NSP-2 and SP, which are also linear in nature.

This model is represented by the DAG in Figure 7(b). y_{A1} and y_{A2} are PCI observations of pavements belonging to category A. x_{A1} and x_{A2} are corresponding pavement ages (the explanatory variable). α_A and β_A are the intercept and age effect for pavements belonging to category A. For the linear model specified by NSP-1, η_{A1}, the unobserved mean of y_{A1}, is calculated as the linear combination of all the incoming nodes: $\alpha_A + \beta_A * x_{A1}$ and $\eta_{A2} = \alpha_A + \beta_A * x_{A2}$. α_A and β_A contribute to all data in category A. The same applies to data in category B, except that they use a separate set of parameters, α_B and β_B. As a result, data and variables for category A and category B are put into separate boxes and no link exists between them.

NSP-2

As each street segment may have its own characteristics, model NSP-2 refines the categories in NSP-1 by treating each street as a category itself, e.g., a separate box for each road segment as shown in Figure 7(c). A linear trend is fitted for each street segment. α and β are the global average intercept and age coefficient and these two variables are shared by data in all categories (not shown but contributing to all η_{ij}s in Figure 7(c)). Besides, for each street segment i, ξ_i and u_i are individual street's deviations in intercept and age effect from the global mean. Both ξ_i and u_i are assumed to be independent and identically distributed (i.i.d.) variables (normally distributed, to be specific) and they only contribute to η_{ij} within the same box in Figure 7(c).

The differences between model NSP-1 and NSP-2 not only lie in the numbers of the categories. Furthermore, the intercepts and age effects in model NSP-1 are allowed to vary without constraints, while these parameters in NSP-2 have to satisfy global normal distribution constraints, controlled by precision variables τ_u and τ_ξ. This is because, as the categories become finer, fewer data points exist for each category and regression coefficients will be significantly affected by errors in the data points. To prevent unrealistically large or small intercepts and age effects from being obtained, global constraints are thus imposed to limit their variation ranges. It will be shown in the coming section that the spatial model addresses the same issue, but with a spatially-correlated parameter.

SP

As there are more than 8,000 street segments in the cleaned dataset, model NSP-2 also includes thousands of parameters. However, most of the additional parameters (ξ_i and u_i) are random effects that serve to improve the model fit without revealing specific reasons or patterns. In comparison, model SP partitions the street level age effect into two parts: the spatially-structured v_i and spatially-unstructured u_i. This is shown graphically in Figure 7(d), where η_{ij}, now having six parent nodes (α and β not shown for clarity of the Figure), is calculated as $\alpha + \xi_i + (\beta + u_i + v_i) * x_{ij}$.

The spatially-structured v_i varies smoothly across the space and makes clusters of road segments based on their degradation rates. Specifically, v_i is assumed to follow the 'Besag' specification (Equation (5)), with mean value equals to the average of the spatial components of its neighbours. This is the unique feature and an advantage of the spatial model, which is to "borrow information/strength from neighbours". Neighbours are defined as adjacent road segments. The more neighbours street segment i has, the smaller the variance of v_i. Similar to NSP-2, the spatially-unstructured random effects in SP (ξ_i and u_i) are also subjected to the global distribution constraints. The spatially-structured v_i, on the contrary, can be viewed as localised constraints on the parameter values.

RESULTS

Parameter estimations for the degradation models are carried out in software R 3.4.1 (R Core Team, 2017). Priors are

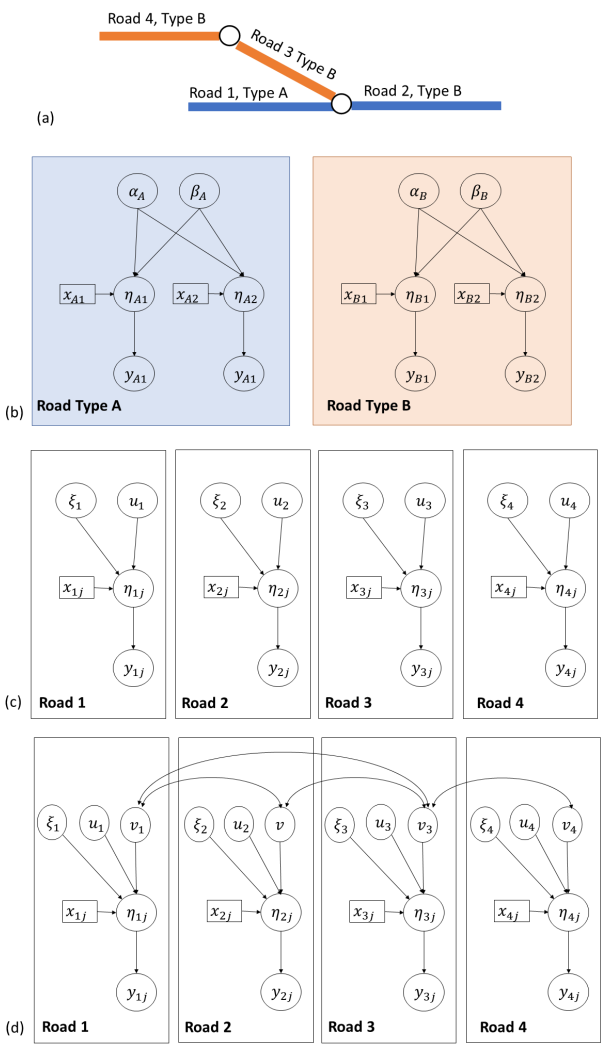

Fig. 7. Graphical models of road degradation. Symbols are consistent with definitions in Equation (1)-(5) and Table 3. For clarity, random noises are not shown in the graphical models. Global level variables (α, β in model NSP-2 and SP, as well as the hyperparameters) are not shown, either. (a) An example network made of 4 road segments and 2 road type categories; (b) NSP-1: coarse categorisation based on road type category; (c): NSP-2: fine categorisation based on individual roads; (4) SP: spatial models with correlated parameters between neighbouring road segments.

specified as the following: for α, the PCI of newly constructed pavement, its physical meaning limits its value to be close to 100. A normal prior with large variance $N(0, 0.0001^{-1})$ is adopted for α. With sufficient data, it is expected that the prior is only weakly-informative, and the posterior distribution will be much narrower than the prior. The same rationale applies to β, the PCI degradation rate, whose actual value is estimated to be a small negative number around -5 to 0, and $N(0, 0.0001^{-1})$ is again chosen as the prior. The hyperparameters τ_ξ, τ_u, τ_v and τ_g are "precision" parameters that are mathematically constrained to be positive. So the Gamma distribution with large variance, $Gamma(1, 0.0005)$, is used as their priors. The Gamma distribution is parameterised with the shape and rate parameters, while the normal distribution is parameterised with mean and variance (inverse of precision), same as the parameterization used in the Model section.

Resulting street-level age-zero condition and degradation rate under the above specified priors are shown in Figure 8 as maps. Moreover, Table 4 provides detailed numerical summaries of the results, including (1) values or distributional characters of the regression coefficients α, β, xi, u and v; (2) the root-mean-square errors (RMSE) on the training and the testing datasets; and (3) the Deviance Information Criteria (DIC) for comparing Bayesian models (Spiegelhalter *et al.*, 2002), which will be explained in detail later in this section.

Prior specifications in INLA may have significant impacts on regression results. Also, priors affect model complexity: the wider the prior is, the more complex (and undesirable) the model becomes. To test whether the results and conclusions still hold under different priors, a sensitivity analysis is carried out and presented at the end of this section.

NSP-1

In NSP-1, regression coefficients (α and β) are obtained based on street type category and the resulting degradation trends are plotted alongside the data in Figure 9. Residential roads (type "*R", the rightmost column in Figure 9) are found to have the lowest degradation rates across all surface types, probably due to the less heavy traffic they carry. Streets with asphalt overlaid surface (type "OA" and "OR", Figure 9(d) and (f)) have the most extreme degradation rates: the yearly PCI change for "OA" roads is as fast as -4.69; while for "OR" roads, it is as slow as -0.43. This may be the consequence of the small numbers of observations for these two types of roads in the dataset.

Additionally, NSP-1 results are presented in different forms as in Figure 8(a), (d), Table 4 (under column NSP-1) and Figure 10(a), (b) (leftmost clusters). They will be compared and discussed with the other two models.

NSP-2

Model NSP-2 fits a linear trend for each street segment. Results suggest that on average the initial PCI condition is 91.62 and drops by 1.83 every year after. The street-level initial conditions and degradation rates are shown as maps in Figure 8(b) and (e).

Additionally, Figure 10 is provided for more visual and detailed comparison of the results. In this figure, each point stands for the regression coefficient for a group or a street segment. The points are clustered and coloured based on street types. Black horizontal bars mark the locations of the 10th, 20th, ..., 90th percentiles for each group. Comparing NSP-2 results with those from NSP-1, it can be seen that the regression coefficients are scattered even within the same street category. For example, in NSP-2, the 30th percentile street-level degradation rates of Portland cement concrete, residential streets (type "PR") is -1.33, while the 70th percentile degradation rate of the same type of street is -1.80, almost 35% faster. Simple group-level results as in NSP-1 cannot adequately capture the individual variations in degradation trends.

SP

Model SP is a spatial extension of NSP-2 that partitions the street-specific degradation rate into two parts: the spatially structured v_i and the spatially unstructured u_i. Maps showing the resulting street-level coefficients from model SP are given by Figure 8(c) and (f). The resulting street-level initial condition map is similar to that of NSP-2, possibly because the intercepts are treated as spatially-unstructured in both models. However, maps of the degradation rates are considerably different: in NSP-2, degradation rates are estimated largely based on individual road segments. In comparison, in SP the regressions are coordinated between several street segments within the defined neighbourhood. The degradation rate map from model NSP-2 does not exhibit any special structure or

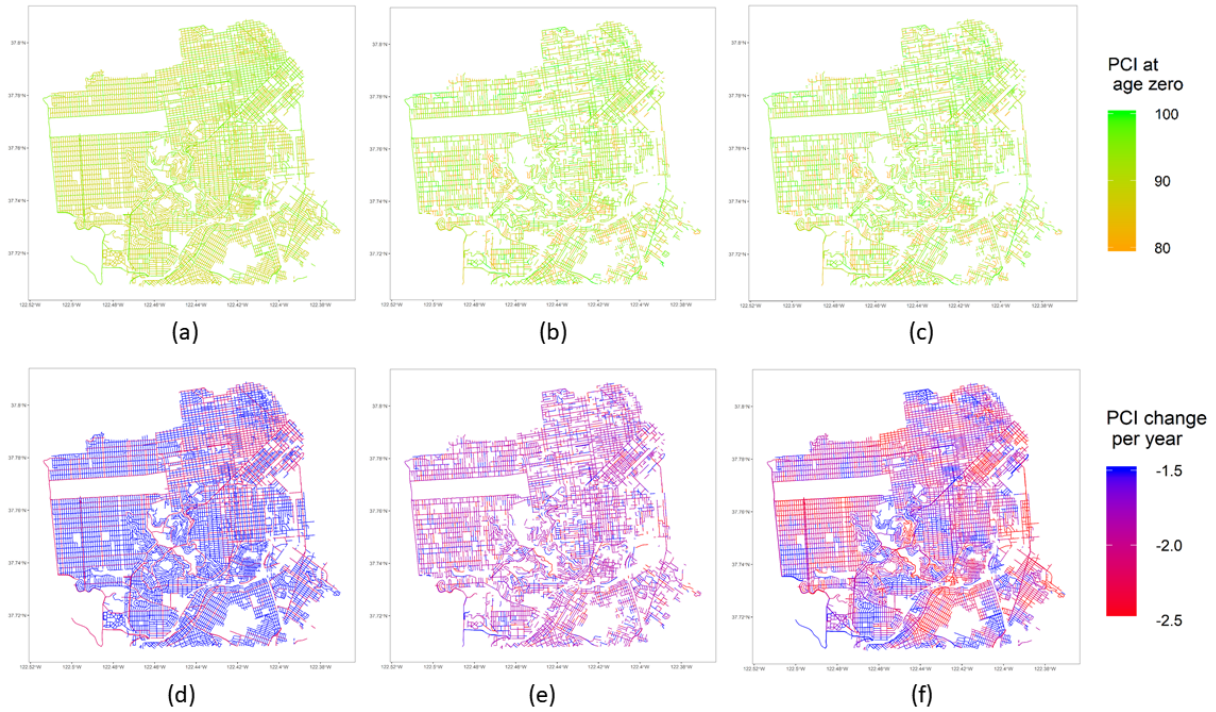

Fig. 8. Map view of regression coefficient results. (a) NSP-1: α; (b) NSP-2: $\alpha + \xi_i$; (c) SP: $\alpha + \xi_i$; (d) NSP-1: β; (e) NSP-2: $\beta + u_i$; (f) SP: $\beta + u_i + v_i$

Table 4. Results

	NSP-1	NSP-2	SP
Intercept	CA: 96.10 CC: 94.11 CR: 87.94 PA: 96.65 PC: 95.85 PR:96.10 OA: 92.29 OR: 86.19	global mean α: 91.62 individual deviation ξ_i: { 1st Quantile: -2.15 Median: 1.79 3rd Quantile: 3.88 }	global mean α: 91.70 individual deviation ξ_i: { 1st Quantile: -2.28 Median: 1.93 3rd Quantile: 3.98 }
Age effect	CA: -2.16 CC: -2.00 CR: -1.41 PA: -1.48 PC: -1.72 PR: -1.30 OA: -4.69 OR: -0.43	global mean β: -1.83 individual deviation u_i: { 1st Quantile: -0.08 Median: 0 3rd Quantile: 0.08 }	global mean β: -1.86 individual deviation: - spatially unstructured u_i { 1st Quantile: -0.008 Median: 0 3rd Quantile: 0.003 } - spatially structured v_i { 1st Quantile: -0.22 Median: 0.02 3rd Quantile: 0.23 }
Train RMSE[1]	12.49	8.56	8.48
Test RMSE	12.42	10.33	10.26
DIC[2]	312633.89	298193.93	297258.12

[1]RMSE: root-mean-square error
[2]DIC: Deviance Information Criterion

pattern (Figure 8(e)), while for model SP, it shows regions of high (in red) and low degradation rates (in blue) (Figure 8(f)). This spatial pattern can be further studied to reveal underlying causes of the differences in degradation rates.

To compare the spread/distributional characters of the regression results from model NSP-2 and SP, Figure 10 is again used. In Figure 10(a), the variations of the intercepts are similar based on model NSP-2 and SP. In Figure 10(b), the resulting degradation rates from model SP are further divided into two parts: "SP-nonspatial" only shows the non-spatial components (i.e., $\beta + u_i$), while "SP-spatial only" shows the spatial components (i.e., $\beta + v_i$). The variation range of v_i is significantly larger than u_i. In other words, a large part of the individual variations in degradation rates are explained by the spatially-structured component.

Model Comparison Using RMSE and DIC

The last three rows in Table 4 give metrics for model comparison. Among them, the root-mean-square-errors (RMSE) of the training and testing datasets are used to compare the fitting and

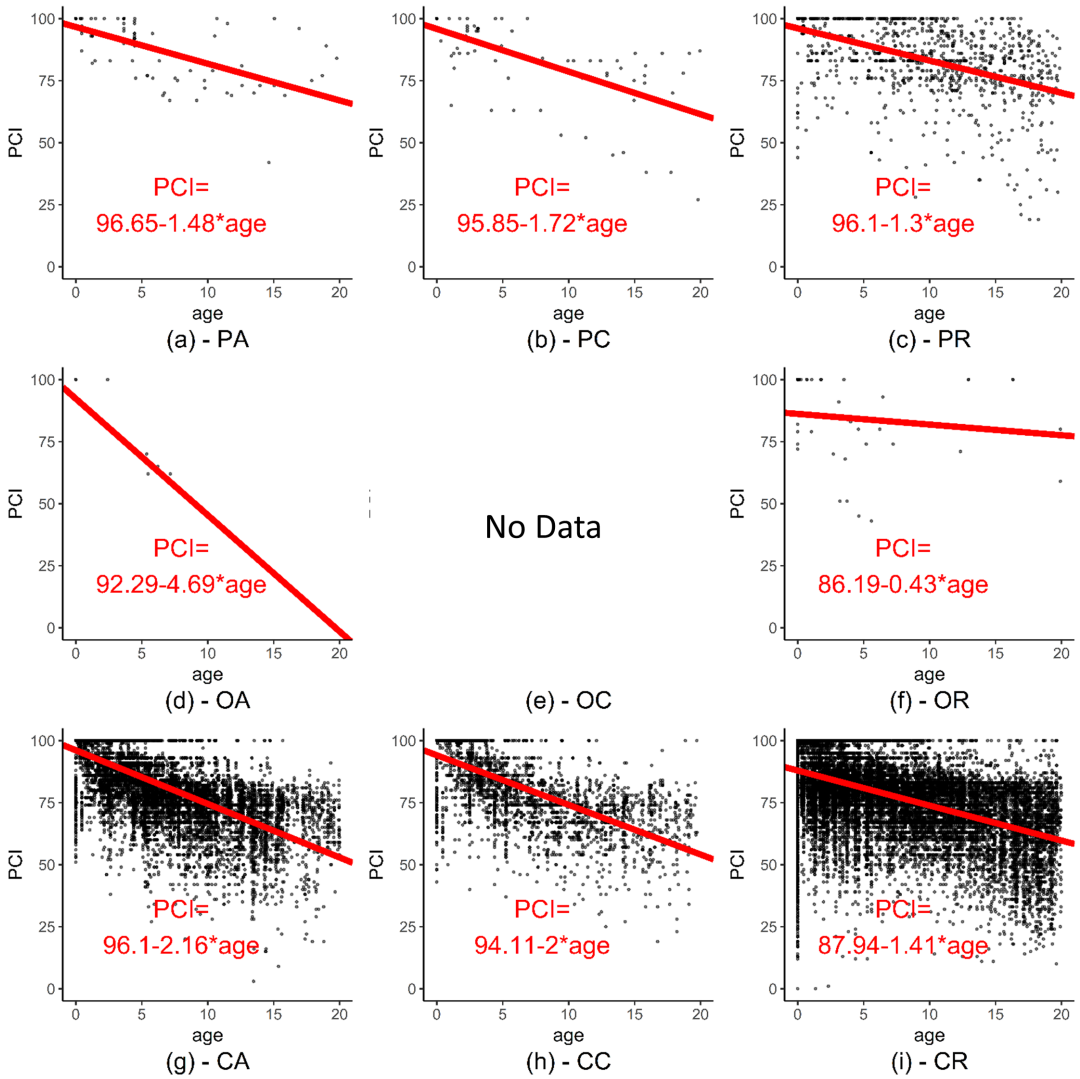

Fig. 9. Regression results from model NSP-1. See Table 2 for meanings of abbreviations

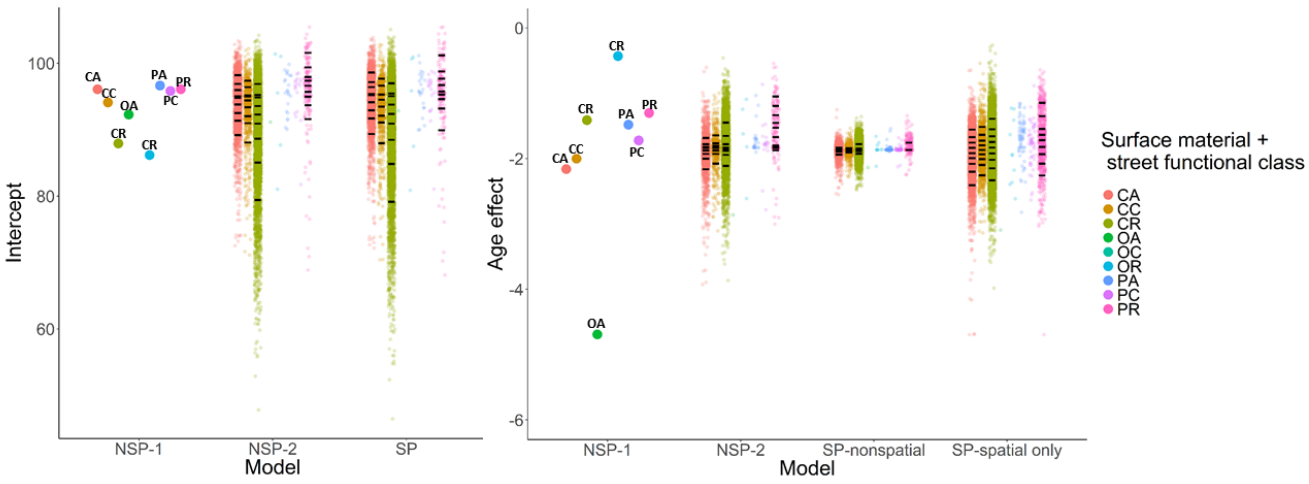

Fig. 10. Resulting intercepts and age effects from different models. See Table 2 for meanings of abbreviations: (a) intercepts; (b) age effects.

predicting abilities of the models. NSP-1, due to its oversimplified structure, has the worst fitting/predicting performance. In fact, it underfits the data, as the testing RMSE (12.42) is about the same as the training RMSE (12.49). NSP-2 performs better than NSP-1, with training RMSE (8.56) and testing RMSE (10.33) both being smaller. The RMSE on the testing dataset is

slightly higher than the training RMSE, but not large enough to be considered as overfitting. Model SP has the smallest training RMSE (8.48) and testing RMSE (10.26) among all three models. Compared with NSP-2, the improvements in fitting and predicting accuracy are not a significant advantage of model SP. The most important strength of model SP is that it has identified regions of high degradation rates. In fact, the spatial component is rather dominant in the total variability of degradation rates based on model SP (10(b)). If the pavement degradation rates do not possess spatial features, results would be expected that the values of the spatial component v_i being closer to zero for all roads. In other words, as the data size for individual pavement is small, estimating its degradation rate is greatly affected by outliers (measurement errors). Model NSP-2 addresses this through identical and independent prior constraints on the parameters, while model SP introduces spatially correlated parameters. The spatial component is found to be dominant, also proving that the spatially correlated constraints is a reasonable problem-specific adaptation of the independent constraints.

Deviance Information Criterion (DIC) is another metric to compare Bayesian models. It is calculated by using either of the formula below (Spiegelhalter *et al.*, 2014):

$$DIC = D(\bar{\theta}) + 2p_D \tag{11}$$

$$DIC = \overline{D} + p_D \tag{12}$$

where D (deviance) is a goodness-of-fit statistics equalling to $-2log(likelihood)$. Smaller deviance indicates a better fit to the data. $D(\bar{\theta})$ is the deviance at posterior means (a classical point-wise measure of model fit) and $\overline{D}$ is the posterior mean deviance (a Bayesian measure of model fit). $p_D = \overline{D} - D(\bar{\theta})$ is the effective number of parameters and reflects the complexity/degree of "overfitting" of the posterior distributions. p_D is included in DIC to penalise complex models. DIC combines the goodness-of-fit measure (D) and the effective number of parameters (p_D), thus reflecting both model fit and complexity. Smaller DIC is better as it indicates a more desirable balance of fit and complexity. The absolute value of DIC is not meaningful and models are compared based on their differences in DIC. From Table 4, SP has the smallest DIC and is the preferred choice among the three models.

Prior Sensitivity Analysis

The sensitivity of Bayesian results on the choice of priors have been discussed in many previous studies (Gelman, 2006; Andrade & Teixeira, 2015). For multi-level or other complex models, even the flat, uninformative uniform priors can become restrictive and informative on transformed parameters. Thus it is important to test a diverse range of prior distributions and to see whether the same conclusion can be reached under different priors. In this study, priors are specified for the following parameters: the global intercept α, the global age effect β, the global precision τ_g, and precisions for street level coefficients τ_ξ, τ_u and τ_v. As α, β and τ_g are global variables, there are sufficient amounts of data to lead to accurate posterior estimations (Gelman, 2006). So only τ_ξ, τ_u and τ_v (in model NSP-2 and SP) are included in the sensitivity analysis.

Table 5 lists the prior combinations used in the sensitivity analysis. Gamma distribution is the usual choice of prior for precision parameters. Four Gamma priors with different distributional characters (labeled A, B, C and D) are tested first. It is possible to use other probability distributions as priors. However, as some streets only have $2 \sim 3$ condition observations in the study period, uniform prior becomes too uninformative that the INLA process fails to complete (Ferkingstad & Rue, 2015). As a substitute, normal priors with large variances (labeled E, F and G) are tested instead.

Figure 11 shows the resulting posterior distributions of τ_ξ, τ_u and τ_v under different prior specifications. Except for τ_u in model SP (Figure 11(c)), the posteriors do not differ much under different priors. For τ_u in model SP, although its mean and variance are sensitive to the prior specifications, its magnitude is almost always larger than τ_v, implying that the spatial effect v still has larger variance ($1/\tau_v$), thus explaining the majority of the individual deviations in degradation rates. Figure 12 as well as the last two columns in Table 5 shows the DIC values for model NSP-2 and SP under different priors. Among the 7 prior choices, the DIC of the spatial model SP is almost always smaller than the non-spatial model NSP-2, indicating the better performance of the spatial model in general.

DISCUSSIONS

Limitations of the Study

A weakness in this study, as shown in the "Results" section, is that for all the three models presented, their training and testing errors are around 10 PCI. This is possibly below the accuracy requirement for asset management. A limitation in the study is that degradations are only modelled linearly with age. Linear models are adopted because they show the key trends more directly than other complex models. But the downside is that the model fit would be compromised. The PCI data used in this study are collected from visual surveys with large variabilities (Tan & Cheng, 2014). The large RMSEs in all three models are likely due to that their simple forms cannot fit the variability (or errors) in the measurement. Nevertheless, the models are still sufficient to demonstrate the advantages of the spatial model.

Advantages of the Spatial Model

For this case study of modelling pavement degradation in San Francisco, the spatial model only wins by a slender lead in terms of accuracy. But the real advantages of the spatial model are within the analysis: first of all, it is able to estimate the degradation parameters for road sections with missing or erroneous observations by borrowing information from adjacent sections, while the richness in the spatial information is lost in non-spatial models. Moreover, it can visually illustrate regions where pavements degrade faster than average. These regions do not necessarily have the worst pavement condition, but they may need maintenance more often in the long term. Local engineers can be consulted, or site investigations conducted, as for the underlying causes. The latter makes spatial models particularly useful in the real practice, as it can assist asset managers to narrow down their attention to a smaller region.

Network-wide Understanding and Smart Infrastructure Management

The spatial pavement degradation model proposed in this study is closely related to the recent advances in the field of Smart Infrastructure and Management. The spatial modelling is built upon two decades of continuous records of city-scale pavement condition data. Such input data are premised on advanced sensing and digital data inventory technologies for pavement infrastructures. On the other hand, the spatial pavement degradation model is also an example of how interdisciplinary data analysis techniques can contribute to the management of smart infrastructures. As a basis, it addresses the imperfections (measurement errors and missing predictors) in pavement condition data and identifies critical regions where pavements tend to age faster. Such results can promote local engineers to conduct more informed inspections/site investigations, eventually making more effective asset management decisions.

Table 5. Prior combinations in the sensitivity analysis

Label	τ_ξ, τ_u and τ_v	DIC of model NSP-2	DIC of model SP
A	$Gamma(1, 0.0005)$	298193.9	297258.1
B	$Gamma(0.1, 0.1)$	297831.0	297384.3
C	$Gamma(0.01, 0.01)$	297890.1	297726.3
D	$Gamma(0.001, 0.001)$	298159.3	297474.0
E	Inverse truncated normal, equivalent to the standard deviation $\sigma = 1/sqrt(\tau) \sim Normal(0, 0.01)$	297972.8	297836.7
F	Inverse truncated normal, equivalent to the standard deviation $\sigma = 1/sqrt(\tau) \sim Normal(0, 0.0001)$	297850.2	298587.7
G	Inverse truncated normal, equivalent to the standard deviation $\sigma = 1/sqrt(\tau) \sim Normal(10, 0.0001)$	298500.9	297288.5

Note: as above, $N(a, b)$ is normal distribution parameterized by mean a and precision b. $Gamma(c, d)$ is Gamma distribution parameterized by shape c and rate d

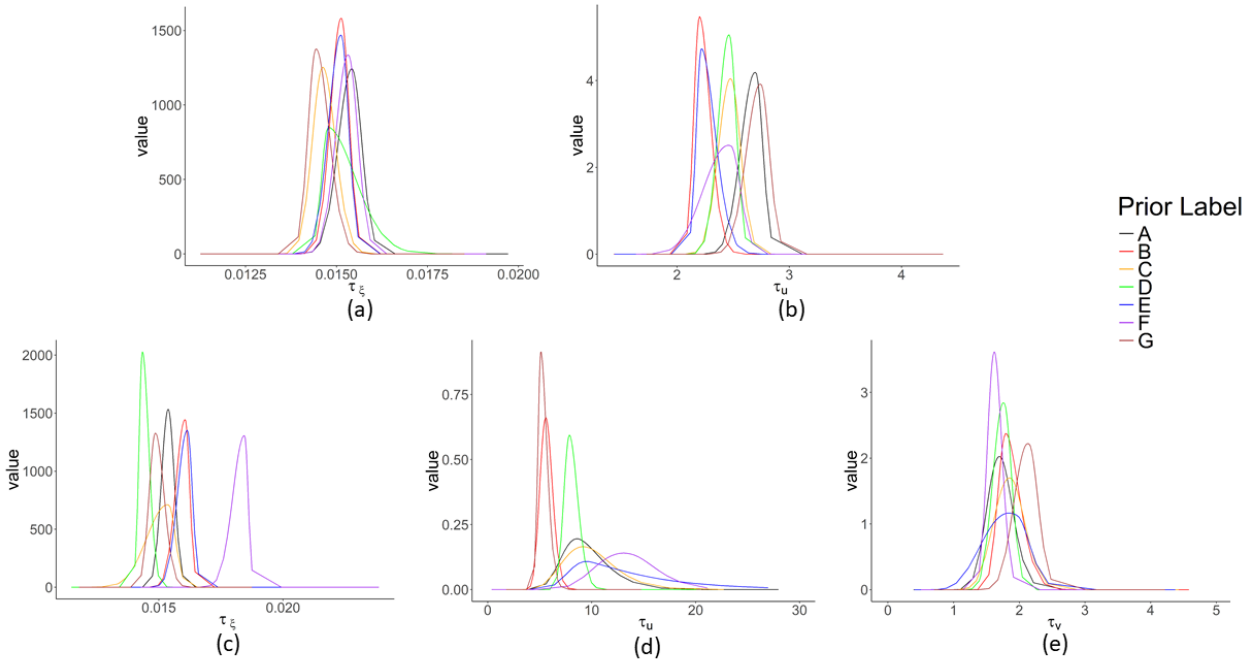

Fig. 11. Posterior distributions under different priors. (a) τ_ξ of model NSP-2; (b) τ_u of model NSP-2; (c) τ_ξ of model SP; (d) τ_u of model SP; (e) τ_v of model SP.

FUTURE WORK

In the future work, more sophisticated spatio-temporal models will be experimented on the pavement degradation dataset. Specifically, convolutional-LSTM has shown promising performance in modeling spatio-temporal events, such as precipitation nowcasting and taxi demand forecasting (Xingjian *et al.*, 2015; Yao *et al.*, 2018). These experiments will be carried out to test their abilities in reducing the modelling errors.

Also, the model evaluation metrics used in this current study (RMSE and DIC) do not fully reflect the need in the real pavement management practice. Other metrics, such as asymmetric loss functions to account for over-predicting and under-predicting, will be incorporated.

The application of spatial model will be further illustrated with similar case studies. Acknowledging that pavement degradation is a spatial process, future case studies will explore whether focusing and investing in critical pavement sections identified by spatial models will achieve cost benefits and serve to improve future pavement conditions in the long run.

Furthermore, the current study on degradation modelling will be extended into asset management and decision making. This will be done through a series of simulation experiments that links pavement degradation with a city-scale traffic model, in order to study the feedback effect of different maintenance strategies.

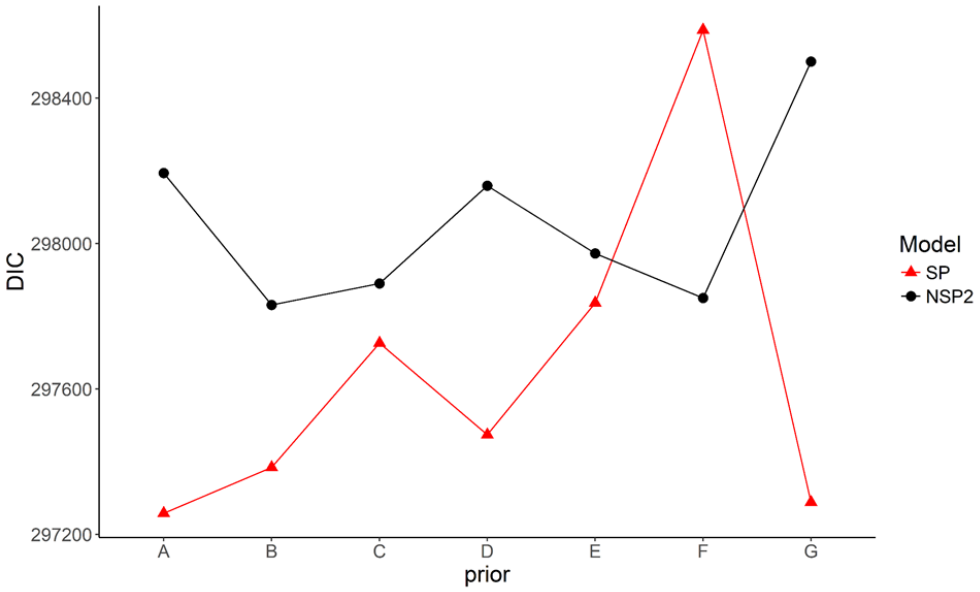

Fig. 12. Resulting DIC of model NSP-2 and SP under different priors.

SUMMARY

This paper incorporates the concept of spatial dependency to the analysis of the ageing of pavements. A spatial model is proposed where the pavement degradation rate of a street segment is determined by its degradation history as well as the degradation history of its neighbouring segments. Two non-spatial models are also included for comparison. The approximation based, efficient Bayesian INLA method is used for parameter inference. Built upon more than two decades of pavement condition survey data collected from the San Francisco road network, it is found that the spatial model is more preferred than the non-spatial models from a Bayesian model selection perspective. The most important advantage of the spatial model is to reveal~~The spatial model also has the advantage of revealing~~ regions where streets with high or low degradation rates cluster. However, it is still necessary for the spatial modelling methodology to be tested on a wider variety of datasets, scenarios, as well as to reduce the modelling errors by incorporating more features or non-linear effects~~datasets and model forms~~. The spatial models can contribute to the improvements of degradation modelling by extracting out the spatially correlated effects, which is likely to be caused by spatially correlated factors such as microclimate, traffic and material continuity~~predictions or yield more information in more application cases~~. The improved pavement degradation model can then be utilised to organise targeted inspections, to investigate the underlying causes of degradation in vulnerable regions, ~~to evaluate the system-level environmental costs~~ and to benefit asset management activities by supporting system-level maintenance planning.

ACKNOWLEDGEMENTS

The authors would like to thank Dr Ruchi Choudhary, Gerard Casey and Dr Krishna Kumar for their help in this work. Also, the authors would like to thank the San Francisco Department of Public Work and DataSF for making the pavement condition data available and the R-INLA project for providing the efficient analysis tools.

REFERENCES

Alaswadko, N., Hassan, R., Meyer, D. & Mohammed, B. (2019). Modelling roughness progression of sealed granular pavements: a new approach. *International Journal of Pavement Engineering* **20**, No. 2, 222–232, doi:10.1080/10298436.2017.1283689, URL https://doi.org/10.1080/10298436.2017.1283689, https://doi.org/10.1080/10298436.2017.1283689.

Aljoufie, M., Zuidgeest, M., Brussel, M., van Vliet, J. & van Maarseveen, M. (2013). A cellular automata-based land use and transport interaction model applied to Jeddah, Saudi Arabia. *Landscape and Urban Planning* **112**, 89 – 99, doi:10.1016/j.landurbplan.2013.01.003, URL http://www.sciencedirect.com/science/article/pii/S0169204613000042.

Andrade, A. R. & Teixeira, P. F. (2015). Statistical modelling of railway track geometry degradation using hierarchical bayesian models. *Reliability Engineering & System Safety* **142**, 169–183, doi:10.1016/j.ress.2015.05.009.

Anyala, M., Odoki, J. & Baker, C. (2014). Hierarchical asphalt pavement deterioration model for climate impact studies. *International Journal of Pavement Engineering* **15**, No. 3, 251–266, doi:10.1080/10298436.2012.687105.

Baller, R. D., Anselin, L., Messner, S. F., Deane, G. & Hawkins, D. F. (2001). Structural covariates of U.S. county homicide rates: Incorporating spatial effects. *Criminology* **39**, No. 3, 561–588, doi:10.1111/j.1745-9125.2001.tb00933.x.

Benbow, E., Wright, A., Dhillon, N., Harrington, M., Nesnas, K., Spong, C. & Cartwright, R. (2017). Development of SCANNER and UKPMS: Task 1, 2 and 3. *Technical Report PPR816 & PPR817*, Transport Research Laboratory Limited, Berks, UK.

Besag, J., York, J. & Mollié, A. (1991). Bayesian image restoration, with two applications in spatial statistics. *Annals of the institute of statistical mathematics* **43**, No. 1, 1–20, doi:10.1007/BF00116466.

Blangiardo, M. & Cameletti, M. (2015). Bayesian computing. In *Spatial and spatio-temporal Bayesian models with R-INLA*, Ch. 4, Chichester, UK: John Wiley & Sons, pp. 75–125.

Blangiardo, M., Cameletti, M., Baio, G. & Rue, H. (2013). Spatial and spatio-temporal models with R-INLA. *Spatial and Spatio-temporal Epidemiology* **4**, 33 – 49, doi:10.1016/j.sste.2012.12.001, URL http://www.sciencedirect.com/science/article/pii/S1877584512000846.

Chen, C., Zhang, S., Zhang, G., Bogus, S. M. & Valentin, V. (2014). Discovering temporal and spatial patterns and characteristics of pavement distress condition data on major corridors in New Mexico. *Journal of Transport Geography* **38**, 148 – 158, doi:10.1016/j.jtrangeo.2014.06.005, URL http://www.sciencedirect.com/science/article/pii/S0966692314001197.

Croissant, Y., Millo, G. *et al.* (2008). Panel data econometrics in R: The plm package. *Journal of Statistical Software* **27**, No. 2, 1–43, doi:10.18637/jss.v027.i02.

Deshmukh, M. M. (2010). *Development of equations to determine the increase in pavement condition due to treatment and the rate of decrease in condition after treatment for a local agency pavement network*. Master's thesis, Texas A & M University, URL http://hdl.handle.net/1969.1/ETD-TAMU-2009-05-317.

Dormann, C. F., McPherson, J. M., Arajo, M. B., Bivand, R., Bolliger, J., Carl, G., Davies, R. G., Hirzel, A., Jetz, W., Kissling, D. W., Khn, I., Ohlemller, R., Peres-Neto, P. R., Reineking, B., Schrder, B., Schurr, F. M. & Wilson, R. (2007). Methods to account for spatial autocorrelation in the analysis of species distributional data: a review. *Ecography* **30**, No. 5, 609–628, doi:10.1111/j.2007.0906-7590.05171.x.

Ferkingstad, E. & Rue, H. (2015). Improving the INLA approach for approximate Bayesian inference for latent Gaussian models. *Electronic Journal of Statistics* **9**, No. 2, 2706–2731, doi:10.1214/15-EJS1092.

Ferreira, A., de Picado-Santos, L., Wu, Z. & Flintsch, G. (2011). Selection of pavement performance models for use in the Portuguese PMS. *International Journal of Pavement Engineering* **12**, No. 1, 87–97, doi:10.1080/10298436.2010.506538.

Ferreira, A., Picado-Santos, L. & Antunes, A. (2002). A segment-linked optimization model for deterministic pavement management systems. *International Journal of Pavement Engineering* **3**, No. 2, 95–105.

Gao, L. & Zhang, Z. (2012). Approximation approach to problem of large-scale pavement maintenance and rehabilitation. *Transportation Research Record: Journal of the Transportation Research Board* , No. 2304, 112–118.

Gelman, A. (2006). Prior distributions for variance parameters in hierarchical models (comment on article by Browne and Draper). *Bayesian analysis* **1**, No. 3, 515–534, doi:10.1214/06-BA117A.

Gelman, A. & Hill, J. (2006). *Data analysis using regression and multilevel/hierarchical models*. Analytical Methods for Social Research, Cambridge University Press, doi:10.1017/CBO9780511790942.

Golabi, K., Kulkarni, R. B. & Way, G. B. (1982). A statewide pavement management system. *Interfaces* **12**, No. 6, 5–21.

Haider, S. W., Baladi, G. Y., Chatti, K. & Dean, C. M. (2010). Effect of frequency of pavement condition data collection on performance prediction. *Transportation Research Record* **2153**, No. 1, 67–80.

Handcock, M. S. & Wallis, J. R. (1994). An approach to statistical spatial-temporal modeling of meteorological fields. *Journal of the American Statistical Association* **89**, No. 426, 368–378, doi:10.2307/2290832, URL http://www.jstor.org/stable/2290832.

Jahanbakhsh, S., Gao, L. & Zhang, Z. (2016). Estimating spatial dependence associated with deterioration process of road network. *Technical Report 16-6179*, Transport Research Board, Washington DC, USA.

Johnson, K. D. & Cation, K. A. (1992). Performance prediction development using three indexes for north dakota pavement management system. *Transportation Research Record* , No. 1344.

Lavine, M. L. & Hodges, J. S. (2012). On rigorous specification of ICAR models. *The American Statistician* **66**, No. 1, 42–49, doi:10.1080/00031305.2012.654746.

Lichstein, J. W., Simons, T. R., Shriner, S. A. & Franzreb, K. E. (2002). Spatial autocorrelation and autoregressive models in ecology. *Ecological Monographs* **72**, No. 3, 445–463, doi:10.1890/0012-9615(2002)072[0445:SAAAMI]2.0.CO;2.

McQueen, J. & Timm, D. (2005). Part 2: Pavement monitoring, evaluation, and data storage: Statistical analysis of automated versus manual pavement condition surveys. *Transportation Research Record: Journal of the Transportation Research Board* , No. 1940, 53–62.

Morosiuk, G., Riley, M. & Odoki, J. (2004). Modelling road deterioration and works effects in HDM-4. *Technical report*, World Road Association (PIARC) and The World Bank, Paris, France and Washington DC, US, URL http://www.lpcb.org/index.php/documents/pavement-deterioration/25191-2004-hdm4-pavement-deterioration-and-maintenance

Nunez, M. M. & Shahin, M. Y. (1986). Pavement condition data analysis and modeling. *Transportation Research Record* **1070**, 125–132.

Open Data Commons (2009). ODC Public Domain Dedication and Licence (PDDL). URL http://opendatacom-mons.org/licenses/pddl/1.0.

Ortiz-García, J. J., Costello, S. B. & Snaith, M. S. (2006). Derivation of transition probability matrices for pavement deterioration modeling. *Journal of Transportation Engineering* **132**, No. 2, 141–161, doi:10.1061/(ASCE)0733-947X(2006)132:2(141).

Paterson, W. D. (1987). *Road deterioration and maintenance effects: Models for planning and management*. Washington DC, USA: The Word Bank, URL http://documents.worldbank.org/curated/en/222951468765265396/Road-deterioration-and-maintenance-effects-models-for-

R Core Team (2017). *R: A language and environment for statistical computing*. R Foundation for Statistical Computing, Vienna, Austria, URL https://www.R-project.org/.

Ramirez-Flores, R. A. & Chang-Albitres, C. (2012). A stochastic approach for pavement condition projections and budget needs for the mtc pavement management system. URL http://onlinepubs.trb.org/onlinepubs/conferences/2012/assetmgmt/presentations/Data-A-Ramirez-Flores-Chang-Albitres.pdf.

Rue, H. & Martino, S. (2007). Approximate Bayesian inference for hierarchical Gaussian Markov random field models. *Journal of Statistical Planning and Inference* **137**, No. 10, 3177 – 3192, doi:10.1016/j.jspi.2006.07.016, URL http://www.sciencedirect.com/science/article/pii/S0378375807000845, special Issue: Bayesian Inference for Stochastic Processes.

Rue, H., Martino, S. & Chopin, N. (2009). Approximate Bayesian inference for latent Gaussian models by using integrated nested Laplace approximations. *Journal of the Royal Statistical Society: Series B (Statistical Methodology)* **71**, No. 2, 319–392, doi:10.1111/j.1467-9868.2008.00700.x.

Sadeghi, J., Najafabadi, E. R. & Kaboli, M. (2017). Development of degradation model for urban asphalt pavement. *International Journal of Pavement Engineering* **18**, No. 8, 659–667, doi:10.1080/10298436.2015.1095912, URL https://doi.org/10.1080/10298436.2015.1095912, https://doi.org/10.1080/10298436.2015.1095912.

Saliminejad, S. & Gharaibeh, N. G. (2012). A spatial-Bayesian technique for imputing pavement network repair data. *Computer-Aided Civil and Infrastructure Engineering* **27**, No. 8, 594–607, doi:10.1111/j.1467-8667.2012.00762.x.

Schrödle, B. & Held, L. (2011). A primer on disease mapping and ecological regression using INLA. *Computational statistics* **26**, No. 2, 241–258, doi:10.1007/s00180-010-0208-2.

SF Public Works (2017). Press release: Sf street pavement condition improves for 5th year in a row - 1/3/2017. URL https://sfpublicworks.org/project/press-release-sf-street-pavement-condition-improves-5t

Shahin, M. Y., Darter, M. I. & Kohn, S. D. (1978). Development of a pavement condition index for roads and streets. *Technical Report ADA057148*, Army Construction Engineering Research Laboratory, Champaign, Illinois, USA, URL http://www.dtic.mil/dtic/tr/fulltext/u2/a057148.pdf.

Shahin, M. Y. & Kohn, S. D. (1982). Overview of the'PAVER'pavement management system and economic analysis of field implementing the'PAVER'pavement management system. *Technical report*, Army Construction Engineering Research Laboratory, Champaign, Illinois, USA,

URL http://www.dtic.mil/cgi-bin/GetTRDoc?Location=U2&doc=GetTRDoc.pdf&AD=ADA116311.

Silva, E. A. & Clarke, K. C. (2005). Complexity, emergence and cellular urban models: lessons learned from applying SLEUTH to two Portuguese metropolitan areas. *European Planning Studies* **13**, No. 1, 93–115, doi:10.1080/0965431042000312424.

Spiegelhalter, D. J., Best, N. G., Carlin, B. P. & Van Der Linde, A. (2002). Bayesian measures of model complexity and fit. *Journal of the Royal Statistical Society: Series B (Statistical Methodology)* **64**, No. 4, 583–639, doi:10.1111/1467-9868.00353.

Spiegelhalter, D. J., Best, N. G., Carlin, B. P. & van der Linde, A. (2014). The deviance information criterion: 12 years on. *Journal of the Royal Statistical Society: Series B (Statistical Methodology)* **76**, No. 3, 485–493, doi:10.1111/rssb.12062.

Tan, S. G. & Cheng, D. (2014). *Quality assurance of performance data for pavement management systems*. doi:10.1061/9780784478462.020, URL https://ascelibrary.org/doi/abs/10.1061/9780784478462.020, https://ascelibrary.org/doi/pdf/10.1061/9780784478462.020.

Tierney, L. & Kadane, J. B. (1986). Accurate approximations for posterior moments and marginal densities. *Journal of the American Statistical Association* **81**, No. 393, 82–86, doi:10.1080/01621459.1986.10478240, URL http://amstat.tandfonline.com/doi/abs/10.1080/01621459.1986.10478240.

Vital Signs (2017). Street pavement condition. URL http://www.vitalsigns.mtc.ca.gov/street-pavement-condition.

Wang, G., Frith, D. & Morian, D. (2014). Implementation of PMS at a local level-case study based on StreetSaver®. In *Civil Engineering and Urban Planning III* (Mohammadian, K., Goulias, K., Cicek, E., Wang, J.-J. & Maraveas, C., eds.), London, UK: Taylor & Francis Group, pp. 207–212.

Wu, Z., Flintsch, G. W. & Chowdhury, T. (2008). Hybrid multi-objective optimization model for regional pavement-preservation resource allocation. *Transportation research record* **2084**, No. 1, 28–37.

Xingjian, S., Chen, Z., Wang, H., Yeung, D.-Y., Wong, W.-K. & Woo, W.-c. (2015). Convolutional lstm network: A machine learning approach for precipitation nowcasting. In *Advances in neural information processing systems*, pp. 802–810.

Yao, H., Wu, F., Ke, J., Tang, X., Jia, Y., Lu, S., Gong, P. & Ye, J. (2018). Deep multi-view spatial-temporal network for taxi demand prediction. *arXiv preprint arXiv:1802.08714* .

Zhang, H., Keoleian, G. A. & Lepech, M. D. (2012). Network-level pavement asset management system integrated with life-cycle analysis and life-cycle optimization. *Journal of infrastructure Systems* **19**, No. 1, 99–107.

Zhao, B. & Nagayama, T. (2017). IRI estimation by the frequency domain analysis of vehicle dynamic responses. *Procedia Engineering* **188**, 9 – 16, doi:10.1016/j.proeng.2017.04.451, URL http://www.sciencedirect.com/science/article/pii/S1877705817320039.

CAPTION LIST

Fig 1. Street network in San Francisco, colored by surface type and functional class categories.

Fig 2. PCI records. (a) A histogram of the observation dates; (b) An example of duplicated PCI values in 1992-1994.

Fig 3. A scatter plot of pavement section's PCI versus age.

Fig 4. Data cleaning examples. (a) Removing outliers; (b) Handling potential missing maintenance records.

Fig 5. Numbers of observations per street segment. (a) A spatial view: the darker the street, the more observations available; (b) The histogram.

Fig 6. PCI versus pavement age, grouped by pavement category. Refer to Table 1 for meanings of abbreviations.

Fig 7. Graphical models of road degradation. Symbols are consistent with definitions in Equation (1)-(5) and Table 2. For clarity, random noises are not shown in the graphical models. Global level variables (α, β in model NSP-2 and SP, as well as the hyperparameters) are not shown, either. (a) An example network made of 4 road segments and 2 road type categories; (b) NSP-1: coarse categorisation based on road type category; (c): NSP-2: fine categorisation based on individual roads; (4) SP: spatial models with correlated parameters between neighbouring road segments.

Fig 8. Map view of regression coefficient results. (a) NSP-1: α; (b) NSP-2: $\alpha + \xi_i$; (c) SP: $\alpha + \xi_i$; (d) NSP-1: β; (e) NSP-2: $\beta + u_i$; (f) SP: $\beta + u_i + v_i$.

Fig 9. Regression results from model NSP-1. See Table 1 for meanings of abbreviations.

Fig 10. Resulting intercepts and age effects from different models. See Table 2 for meanings of abbreviations: (a) intercepts; (b) age effects.

Fig 11. Posterior distributions under different priors. (a) τ_ξ of model NSP-2; (b) τ_u of model NSP-2; (c) τ_ξ of model SP; (d) τ_u of model SP; (e) τ_v of model SP.

Fig 12. Resulting DIC of model NSP-2 and SP under different priors.

Table 1. Pavement categories and numbers of street segments in each category.

Table 2. Models.

Table 3. Results.

Table 4. Prior Combinations in the Sensitivity Analysis.